Tomographic study of atomic-scale redistribution of platinum during the silicidation of $Ni_{0.95}Pt_{0.05}$/Si(100) thin films

Praneet Adusumilli,[1] Lincoln J. Lauhon,[1] David N. Seidman,[1,a)] Conal E. Murray,[2] Ori Avayu,[3] and Yossi Rosenwaks[3]
[1]*Department of Materials Science and Engineering, Northwestern University, 2220 Campus Drive, Evanston, Illinois 60208-3108, USA*
[2]*IBM Thomas J. Watson Research Center, Yorktown Heights, New York 10598, USA*
[3]*School of Electrical Engineering, Tel-Aviv University, Tel-Aviv 69978, Israel*

(Received 19 January 2009; accepted 25 February 2009; published online 16 March 2009)

Atom-probe tomography was utilized to study the distribution of Pt after silicidation of a solid-solution $Ni_{0.95}Pt_{0.05}$ thin film on Si(100). Direct evidence of Pt short-circuit diffusion via grain boundaries, Harrison's type-B regime, is found after silicidation to form $(Ni_{0.99}Pt_{0.01})Si$. This underscores the importance of interfacial phenomena for stabilizing this low-resistivity phase, providing insights into the modification of NiSi texture, grain size, and morphology caused by Pt. Platinum segregates at the $(Ni_{0.99}Pt_{0.01})Si/Si(100)$ interface, which may be responsible for the increased resistance of $(Ni_{0.99}Pt_{0.01})Si$ to agglomeration. The relative shift in work function between as-deposited and annealed states is greater for Ni(Pt)Si than for NiSi. © *2009 American Institute of Physics*. [DOI: 10.1063/1.3099970]

Nickel monosilicide is being extensively studied for use as source and drain contacts in complementary metal-oxide semiconductor devices.[1–3] The most challenging issue in integrating this low-resistivity material is its thermal stability. At elevated temperatures (~700 °C), NiSi degrades either via agglomeration or via phase transformation to the higher resistivity $NiSi_2$ phase. Addition of a transition metal, such as Pt, Pd, or Rh, has been shown to reduce the agglomeration of thin NiSi films and increase the formation temperature of $NiSi_2$,[4] and it has been suggested that changes in the bulk free energy due to entropy of mixing can explain this effect.[5,6] We have recently shown that Pd segregates at the $(Ni_{0.98}Pd_{0.02})Si/Si(100)$ heterophase interface with a Gibbsian interfacial excess of 3.4 ± 0.2 atom nm^{-2}, suggesting that the influence of transition metal additives on *interfacial* energies may promote stabilization of $(Ni_{0.98}Pd_{0.02})Si$ at elevated temperatures.[7] It is therefore important to examine in greater detail the three-dimensional (3D) distribution of the alloying elements in $(Ni_{1-x}Pt_x$ or $Pd_x)Si$ thin films to better understand the stabilization of this low-resistivity phase. We report herein on the use of 3D laser-assisted local-electrode atom-probe (LEAP®) tomography to study the atomic-scale distribution of Pt produced by reacting $Ni_{0.95}Pt_{0.05}$ thin films with Si(100). Direct evidence is presented for short-circuit diffusion of Pt via grain boundaries (GBs) in the $(Ni_{0.99}Pt_{0.01})Si$ phase that forms on Si(100), after a 5 s silicidation reaction at 420 °C.

Samples were fabricated by sputter depositing 10 nm thick $Ni_{0.95}Pt_{0.05}$ thin films on undoped Si (100) wafers at room temperature after the removal of the native oxide. A 30 nm thick Co capping layer was deposited without breaking vacuum to serve as an oxidation barrier (Fig. 1). Cobalt was chosen because its evaporation field is similar to that of Ni, facilitating a smooth transition from this capping layer to the experimental region-of-interest. These films were subjected to rapid thermal annealing (RTA) at 420 °C for 5 s to form a low-resistivity Ni monosilicide phase. Specimens for 3D atom-probe tomography (APT) were prepared from blanket structures using a FEI Helios dual-beam focused ion beam (FIB) microscope and an Omniprobe micromanipulator employing the lift-out technique.[8,9] The tips were Ga^+ ion milled to achieve an end radius of ~50 nm. Pulsed picosecond-laser APT was performed for compositional profiling of the thin film with subnanometer scale spatial resolution.[10,11] The analyses were performed at a specimen temperature of 40 ± 0.3 K, a 500 kHz pulse repetition rate, an energy of 0.5 nJ $pulse^{-1}$, an evaporation rate of 0.2% ions $pulse^{-1}$, and a gauge pressure of $<6.6 \times 10^{-9}$ Pa.

Figure 1 describes schematically the thin-film structure before and after RTA processing. The silicidation process involves interdiffusion of Ni, Pt, and Si, and a simultaneous chemical reaction to form the monosilicide phase. The schematic is based on an APT reconstruction of a $50 \times 50 \times 100$ nm^3 analysis volume that reveals sequentially three regions in the thin film: (i) an intermixed region ~35 nm thick, consisting of $Ni_{1-x}Pt_x$, where x varies with distance from the surface, and a Co capping layer; (ii) the Ni mono-

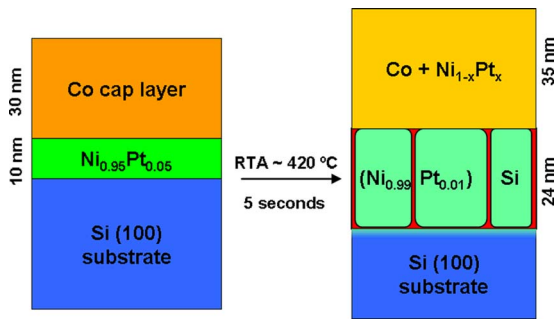

FIG. 1. (Color online) Schematic diagram illustrating the thin-film structure before and after RTA at 420 °C for 5 s. The color red indicates the GBs and shows the columnar nature of the $(Ni_{0.99}Pt_{0.01})Si$ grains with the long axis oriented normal to the thin film's surface.

a)Author to whom correspondence should be addressed. Electronic mail: d-seidman@northwestern.edu.

 © 2009 American Institute of Physics

Downloaded 16 Mar 2009 to 129.105.215.213. Redistribution subject to AIP license or copyright; see http://apl.aip.org/apl/copyright.jsp

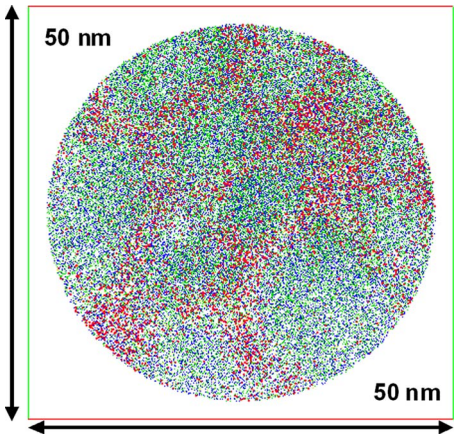

FIG. 2. (Color online) Two-dimensional (2D) top-view projection along the analysis direction of a full 3D reconstruction of 3D atom-probe tomographic data displaying the distribution of elements. Nickel, Si, and Pt atoms are shown in green, blue, and red, respectively. An analysis volume of $50\times50\times5$ nm^3 (4×10^5 atoms) is displayed from the silicide region of the complete reconstruction. Only 25% of the Ni and Si atoms are displayed for clarity.

silicide phase $(Ni_{0.99}Pt_{0.01})Si$, ~24 nm thick; and (iii) the Si(100) substrate. The Pt concentration is quantified using the volume average value within the silicide grains. The thickness of the monosilicide phase is approximately what is anticipated from the consumption of the metal film.[3] The red color in Fig. 1 indicates the GBs associated with the $(Ni_{0.99}Pt_{0.01})Si$ grains, which are columnar in nature (Figs. 2 and 3). A small amount of Co is found in the monosilicide phase and it plays a passive role. Platinum segregates at the $(Ni_{0.99}Pt_{0.01})Si/Si(100)$ interface, which has a Gibbsian interfacial excess of Pt of 0.88 ± 0.01 nm^{-2}.[12] Agglomeration of thin films is believed to be driven by a reduction in the interfacial Gibbs free energy of the NiSi/Si(100) interface as a result of the reduction in the contact area between the phases. The segregation of Pt at the $(Ni_{0.99}Pt_{0.01})Si/Si(100)$ interface reduces its interfacial Gibbs free energy by 8.5 mJ m^{-2},[13] and thereby decreases the thermodynamic driving force for agglomeration of the thin film.

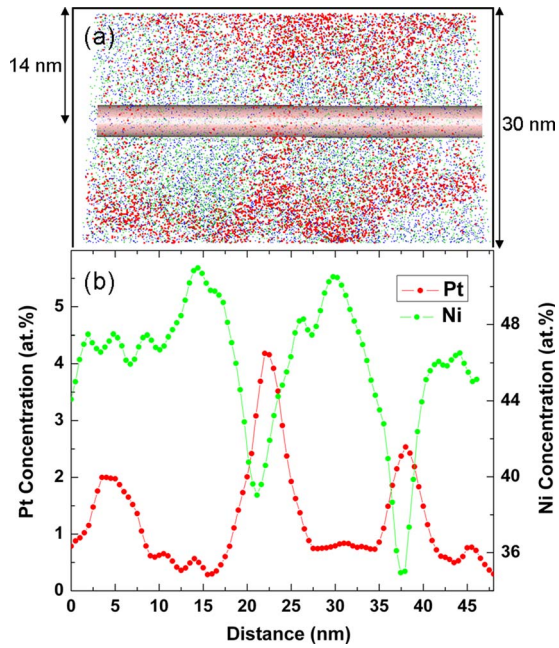

FIG. 3. (Color online) (a) 2D vertical slice along the analysis direction of 3D LEAP tomographic data at a depth of ~15 nm. An analysis volume of $30\times50\times5$ nm^3 (2.88×10^5 atoms) is displayed using the same coloring scheme for atoms (Fig. 2). Only 10% of Ni and Si atoms are displayed for clarity. (b) 1D composition profile of Pt and Ni atoms within the $4\times4\times48$ nm^3 cylindrical volume element placed horizontally across three GBs of the $(Ni_{0.99}Pt_{0.01})Si$ grains as displayed in (a).

Figure 2 displays the top view along the analysis direction of a $50\times50\times5$ nm^3 analysis volume within the silicide region of the film at a depth of ~10 nm from the $(Ni_{1-x}Pt_x+Co)/(Ni_{0.99}Pt_{0.01})Si$ interface. Each dot represents a single atom in the reconstruction: Ni, Si, and Pt are displayed in green, blue, and red, respectively. Platinum atoms are seen decorating the GBs of the $(Ni_{0.99}Pt_{0.01})Si$ phase at a high concentration. Figure 3(a) displays a side view of the Pt distribution associated with $(Ni_{0.99}Pt_{0.01})Si$ grains in a $50\times5\times30$ nm^3 slice of the reconstruction volume showing the monosilicide portion of the film. Figure 3(b) shows one-dimensional (1D) composition profiles of Pt and Ni atoms in a cylindrical analysis volume, placed ~14 nm below the $(Ni_{1-x}Pt_x+Co)/(Ni_{0.99}Pt_{0.01})Si$ interface, which is perpendicular to the GBs of three $(Ni_{0.99}Pt_{0.01})Si$ grains, Fig. 3(a). The significantly greater Pt concentration in the GB region compared to the bulk of the grains implies that short-circuit diffusion is occurring via the GBs of the $(Ni_{0.99}Pt_{0.01})Si$ thin film. GB diffusion of Pt has recently been suggested as occurring in the metal-rich Ni_2Si phase.[14] A concomitant decrease in the Ni concentration profile is observed in the GB region, suggesting that Pt is substituting for Ni, Fig. 3(b). The Pt concentration profile indicates Harrison's type-B regime for short-circuit diffusion along high-diffusivity paths.[15,16] In this case the type-B regime is characterized by (i) volume diffusion from the unreacted $Ni_{1-x}Pt_x$ thin film, (ii) volume diffusion laterally from the GBs into the grains in the $(Ni_{0.99}Pt_{0.01})Si$ region, and (iii) short-circuit diffusion along the GBs. Platinum is found to accumulate at the $(Ni_{1-x}Pt_x+Co)/(Ni_{0.99}Pt_{0.01})Si$ interface, which acts as a source for both volume and GB diffusion, Fig. 3(a). The cylindrical analysis volume [Fig. 3(a)] is placed at a depth greater than the root-mean-square (rms) diffusion distance (~3 nm) of Pt from the surface. The extent of the lateral Pt concentration profile across the $(Ni_{0.99}Pt_{0.01})Si$ grains is dependent on grain size. For smaller grains with diameter $\leq$ ~15 nm, the Pt concentration profiles from adjacent GBs overlap [Fig. 3(b), center grain]. The high spatial resolution available enables direct, precise, and accurate measurements of the lattice (D_l) and GB (D_{GB}) diffusivities at 420 °C. No Pt concentration gradients are found along the GBs, implying that D_{GB}, is significantly greater than D_l. By plotting the $\log_{10}$ (Pt concentration) in the grains versus the distance squared, we obtain a D_l of $4.2\pm1.2\times10^{-19}$ m^2 s^{-1} averaged over ten grains. Utilizing the Whipple–Suzuoka analysis[17,18] at 420 °C, the value of δD_{GB} is 7.3×10^{-26} m^3 s^{-1}, where δ is the GB width. Taking δ to be 0.5 nm implies that $D_{GB}=1.5\times10^{-16}$ m^2 s^{-1}, which is ~350 times greater than D_l. The diffusivity measurements are affected by the simultaneous reaction between Ni and Si to form the nickel monosilicide phase.

The observation of short-circuit diffusion via GBs sheds light on the kinetics of diffusion and has important implications for phase formation and phase retention. Since very little Pt is found inside the $(Ni_{0.99}Pt_{0.01})Si$ grains, we con-

Downloaded 16 Mar 2009 to 129.105.215.213. Redistribution subject to AIP license or copyright; see http://apl.aip.org/apl/copyright.jsp

clude that for the short annealing times employed for source/drain contact fabrication, entropy of mixing arguments *cannot* explain the increased resistance to the formation of $NiSi_2$. The presence of high-diffusivity GB paths makes it possible for Pt to diffuse to the silicide/Si interface even for short annealing times. This may be responsible for the reported modification of the texture of NiSi thin films with Pt additions.[2,3,5,19] In light of the discovery of Pt short-circuit diffusion along GBs, the observed modification of the NiSi grain size[20] and morphology may be explained by solute drag[21] on GBs by Pt.

Additionally, Kelvin probe force microscopy[22–24] was used to measure the work-function (WF) of the fabricated silicide samples. The tip's WF was calibrated before each measurement by measuring its value for *in situ* peeled highly oriented pyrolytic graphite. The unreacted Ni-5 at. % Pt alloy on top was removed using H_2SO_4:H_2O_2 etchants. The WF of the $(Ni_{0.99}Pt_{0.01})Si$ surface was 4.57 ± 0.015 eV. A similar measurement on the as-deposited specimens yielded a WF value of 3.85 ± 0.015 eV. The relative shift in WF between as-deposited and annealed states is greater for Ni(Pt)Si (0.72 ± 0.015 eV) than for NiSi (0.67 ± 0.015 eV). This indicates a desirable increase in WF toward the valence band edge of Si (5.1 eV) with the incorporation of Pt during silicidation. This results in a reduction in the Schottky barrier height of the contact to *p*-type Si and the corresponding contact resistance. The chemical rms roughness of the $(Ni_{0.99}Pt_{0.01})Si/Si(100)$ interface, for a 75 at. % Si isoconcentration surface, is ~1.3 nm. A chemically smooth interface reduces electronic scattering, so that its contact resistance is minimized. It has been shown that a specific contact resistance of $1-2 \times 10^{-8}$ Ω cm^2 is achieved for appropriate doping conditions.[25] In conclusion, the combination and correlation of chemical composition profiling utilizing APT with electrical WF measurements provides a powerful tool for microelectronics researchers.

In summary, we have mapped the subnanometer scale distribution of Pt in Ni monosilicide thin films to ascertain its role in stabilizing the monosilicide film against agglomeration and phase change at elevated temperatures. Direct and quantitative evidence of short-circuit diffusion[26] along the GBs, Harrison's type-B regime, of the nickel monosilicide phase is presented. This might help explain the modification of NiSi texture, grain size, and morphology on the addition of Pt. Consequently, for short annealing times, 5 s in this case, entropy of mixing arguments cannot be used to explain the increase in the $NiSi_2$ formation temperature.[5,6] Platinum is found to segregate at the $(Ni_{0.99}Pt_{0.01})Si/Si(100)$ heterophase interface, and the resulting reduction in the interfacial Gibbs free energy of ~8.5 mJ m^{-2} may explain the increased resistance to agglomeration. The WF of the $(Ni_{0.99}Pt_{0.01})Si$ film's surface shifted toward the Si valence band edge with silicidation and progressive incorporation of Pt into the structure.

This research is supported by Semiconductor Research Corporation, Contract No. 1441.001. Atom-probe tomographic measurements were performed at the Northwestern University Center for Atom-Probe Tomography (NUCAPT), which is managed by Research Assistant Professor D. Isheim. The 3D LEAP tomograph was purchased with funding from the NSF-MRI (Grant No. DMR 0420532) and ONR-DURIP (Grant No. N00014-0400798) programs. The FEI dual-beam FIB was used in the EPIC facility of the NUANCE Center at Northwestern University.

[1] A. Lauwers, J. A. Kittl, M. J. H. Van Dal, O. Chamirian, M. A. Pawlak, M. de Potter, R. Lindsay, T. Raymakers, X. Pages, B. Mebarki, T. Mandrekar, and K. Maex, Mater. Sci. Eng., B **114**, 29 (2004).
[2] C. Lavoie, F. M. d'Heurle, C. Detavernier, and C. Cabral, Microelectron. Eng. **70**, 144 (2003).
[3] C. Lavoie, C. Detavernier, and P. Besser, in *Nickel Silicide Technology*, edited by L. J. Chen (IEE, London, 2004), Vol. 5, pp. 95–151.
[4] C. Lavoie, C. Detavernier, C. Cabral, Jr., F. M. d'Heurle, A. J. Kellock, J. Jordan-Sweet, and J. M. E. Harper, Microelectron. Eng. **83**, 2042 (2006).
[5] D. Mangelinck, J. Y. Dai, J. S. Pan, and S. K. Lahiri, Appl. Phys. Lett. **75**, 1736 (1999).
[6] J. F. Liu, J. Y. Feng, and J. Zhu, Appl. Phys. Lett. **80**, 270 (2002).
[7] Y. C. Kim, P. Adusumilli, L. J. Lauhon, D. N. Seidman, S. Y. Jung, H. D. Lee, R. L. Alvis, R. M. Ulfig, and J. D. Olson, Appl. Phys. Lett. **91**, 113106 (2007).
[8] K. Thompson, D. Lawrence, D. J. Larson, J. D. Olson, T. F. Kelly, and B. Gorman, Ultramicroscopy **107**, 131 (2007).
[9] D. J. Larson, D. T. Foord, A. K. Petford-Long, H. Liew, M. G. Blamire, A. Cerezo, and G. D. W. Smith, Ultramicroscopy **79**, 287 (1999).
[10] D. N. Seidman, Annu. Rev. Mater. Res. **37**, 127 (2007).
[11] T. F. Kelly and M. K. Miller, Rev. Sci. Instrum. **78**, 031101 (2007).
[12] O. C. Hellman, J. A. Vandenbroucke, J. Rüsing, D. Isheim, and D. N. Seidman, Microsc. Microanal. **6**, 437 (2000).
[13] B. W. Krakauer and D. N. Seidman, Acta Mater. **46**, 6145 (1998).
[14] B. Imbert, C. Guichet, S. Bonnetier, S. Zoll, M. Juhel, M. Hopstaken, P. Clifton, and O. Thomas, Microelectron. Eng. **84**, 2523 (2007).
[15] L. G. Harrison, Trans. Faraday Soc. **57**, 1191 (1961).
[16] A. P. Sutton and R. W. Balluffi, *Interfaces in Crystalline Materials* (Oxford University, New York, 1995), pp. 467–481.
[17] R. T. Whipple, Philos. Mag. **45**, 1225 (1954).
[18] T. Suzuoka, J. Phys. Soc. Jpn. **19**, 839 (1964).
[19] C. Detavernier and C. Lavoie, Appl. Phys. Lett. **84**, 3549 (2004).
[20] H. Akutsu, H. Itokawa, K. Nakamura, T. Iinuma, K. Suguro, H. Uchida, M. Tada, Mater. Res. Soc. Symp. Proc. **1070**, 1070–E02–09 (2008).
[21] S. G. Kim and Y. G. Park, Acta Mater. **56**, 3739 (2008).
[22] Y. Rosenwaks, R. Shikler, Th. Glatzel, and S. Sadewasser, Phys. Rev. B **70**, 085320 (2004).
[23] S. Sadewasser, Th. Glatzel, R. Shikler, Y. Rosenwaks, and M. Ch. Lux-Steiner, Appl. Surf. Sci. **210**, 32 (2003).
[24] Th. Glatzel, S. Sadewasser, R. Shikler, Y. Rosenwaks, and M. Ch. Lux-Steiner, Mater. Sci. Eng., B **103**, 138 (2003).
[25] K. Ohuchi, C. Lavoie, C. Murray, C. D'Emic, I. Lauer, J. O. Chu, B. Yang, P. Besser, L. Gignac, J. Bruley, G. U. Singco, F. Pagette, A. W. Topol, M. J. Rooks, J. J. Bucchignano, V. Narayanan, M. Khare, M. Takayanagi, K. Ishimaru, D. G. Park, G. Shahidi, P. Solomon, Tech. Dig. - Int. Electron Devices Meet. **2007**, 1029.
[26] G. Martin and B. Perraillon, *Grain-Boundary Structure and Kinetics* (ASM, Ohio, 1979), pp. 239–276.

Downloaded 16 Mar 2009 to 129.105.215.213. Redistribution subject to AIP license or copyright; see http://apl.aip.org/apl/copyright.jsp